Spin-torque driven magnetization dynamics in a nanocontact setup for low external fields: Numerical simulation study

D. V. Berkov and N. L. Gorn
Innovent Technology Development e.V., Pruessingstr. 27B, D-07745 Jena, Germany
(Received 13 March 2009; revised manuscript received 16 June 2009; published 14 August 2009)

We present numerical simulation studies of the steady-state magnetization dynamics driven by a spin-polarized current in a point-contact geometry for the case of a relatively large contact diameter (D_c=80 nm) and small external field (H=30 Oe). We show that under these conditions the magnetization dynamics is qualitatively different from the dynamics observed for small contacts in large external fields. In particular, the "bullet" mode with a relatively homogeneous mode core, which was the dominating localized mode for small contacts, is not found here. Instead, all localized oscillation modes observed in simulations correspond to different motion kinds of vortex-antivortex (V-AV) pairs. These modes include rotation of pairs with the V-AV distance $d \sim D_c$ and creation/annihilation of much smaller (satellite) V-AV pairs. We also show that for our geometry the Oersted field has a qualitative effect on the magnetization dynamics of a free layer. This effect offers (in principle) a possibility to control magnetization dynamics by a suitable electric contact setup, adjusted to produce a desired Oersted field. Finally, we demonstrate that when the magnetization dynamics of the "fixed" layer—induced by the magnetodipolar interaction with the "free" layer—is taken into account, the threshold current for the oscillation onset is drastically reduced and new types of localized modes appear. In conclusion, we show that our simulations reproduce semiquantitatively several important features of the magnetization dynamics in a point-contact system for low external fields reported experimentally.

DOI: 10.1103/PhysRevB.80.064409 PACS number(s): 85.75.−d, 75.75.+a, 75.40.Gb, 75.40.Mg

I. INTRODUCTION

Magnetization dynamics induced in thin multilayer elements by a spin-polarized current (SPC) is currently one of the most intensively studied topics in the solid-state magnetism. After theoretical predictions[1,2] and first experimental confirmations of this phenomenon[3] it was quickly realized that SPC-induced magnetization excitations and switching represent not only a very interesting phenomenon from the fundamental point of view (see review papers,[4–7] but is also are a very promising candidate for numerous device applications (for recent reviews see Refs. 8–11).

Among various experimental geometries used to study the spin torque induced magnetization dynamics, the so-called point-contact setup (where the current is injected into a multilayer element with lateral sizes in micrometer region via a contact with the diameter $D_c \sim 10-100$ nm) is one of the most interesting designs: it offers a large variety of magnetization oscillation modes, depending on the contact size, applied field strength and direction and magnetic materials used to compose a multilayer element.[12–15] Moreover, one of the desired applications of the SPC-induced dynamics is the construction of *dc*-fed microwave generators, which should output enough power to be applicable in real technical devices. For this application the point-contact setup is especially interesting: there exists—at least in principle—a possibility to synchronize magnetization oscillations induced by several point contacts attached to the same multilayer,[16,17] thus greatly increasing the output power due to the constructive wave interference.

For all these reasons magnetization dynamics in point-contact devices have been the subject of intensive research during the last few years. Already the first quantitatively accurate experimental observation of magnetization oscillation in this geometry[12] posed an intriguing question about the nature of the observed oscillation mode. Namely, the measured oscillation frequency, being below the homogeneous ferromagnetic resonance (FMR) frequency for the magnetic layer studied in Ref. 12 could not correspond to the propagating wave mode predicted for such devices by Slonczewski.[18] Numerical simulations have shown that in such systems at least one *localized* mode type could exist[19] (in addition to the propagating wave), which was independently identified by the analytical theory[20] as a nonlinear "bullet." Further theoretical and numerical studies have proven[21,22] that this "bullet" was indeed the mode observed in the pioneering paper.[12]

Detailed numerical simulations[22,23] have suggested that a much more complicated localized modes, consisting of vortex-antivortex pairs, can exist in point-contact devices. The frequency of these modes, according to our simulation predictions, should be much lower than for the "bullet" mode (not to mention the propagating wave mode), and, should be also nearly current independent.[22] Both features would make these modes very interesting from the point of view of technical application, because such modes would expand the frequency range of SPC-based microwave generators and offer a stability of the generated frequency with respect to current strength fluctuations. Further experimental studies have indeed shown that magnetization oscillations observed in the nanocontact setup in very weak in-plane[14,24] or out-of-plane fields[14,25] cannot correspond to the 'bullet' mode. Due to their very low frequency $f \sim 100-500$ MHz (what is really low for the SPC-induced dynamics), the oscillations observed in Refs. 14 and 25 were attributed to magnetization dynamics governed by the motion of a single vortex (for a strong out-of-plane field in Ref. 25) or vortex-antivortex pairs (in very weak fields[24,26]).

Especially interesting in this context are magnetization oscillations observed in point-contact devices with relatively large contact diameter (~100 nm) and in weak external fields. In such conditions, due to the absence of the stabilizing influence of the external field and relatively large area flooded by a spin-polarized current, strongly inhomogenous magnetization excitations can occur. Indeed, a qualitatively new oscillation mode was found experimentally in,[14] where for a point contact with the diameter ≈60–80 nm, attached to an extended $Co_{90}Fe_{10}/Cu/Ni_{80}Fe_{20}$ multilayer, microwave oscillations with extremely low frequency (down to ~100 MHz) and very weak frequency dependence on the current strength were observed. It was suggested that the observed dynamics can be explained by the generation and movement of a magnetic vortex, but no supporting simulations or analytical theory were reported in Ref. 14.

For all the reasons explained above, we have performed systematic numerical studies of the SPC-induced magnetization excitations for the case, when a point contact with a relatively large diameter is attached to an extended multilayer and the applied field is very weak (some preliminary results of this research have been briefly reported in the last part of our overview[26]). The paper is organized as follows. In Sec. II we describe in detail the simulation methodology, geometry and magnetic parameters of the simulated system. Section III contains the description of our main results: we start with the single-layer system without the Oersted field (Sec III A), proceed with the demonstration of the Oersted field effects (IIIB) and finish our presentation with the analysis of magnetodipolar interaction effects, when the "hard" magnetic layer is included into the simulated system. Section IV contains the comparison of our results with experimental data and numerical simulations of other groups.

II. SIMULATED SYSTEM AND SIMULATION METHODOLOGY

In this paper we intend to study the influence of various physical factors on the magnetization precession induced in the point-contact geometry by a spin-polarized current flowing perpendicular to the magnetic multilayer plane. In contrast to previous numerical simulation studies,[21–23,25,27] we focus our attention on the case where (i) the point-contact diameter D_c is relatively large and (ii) the external field H_{ext} is small compared to the saturation magnetization of the material. As expected from general arguments and confirmed by recent experiments of the NIST group,[14] for this case one expects a qualitatively different magnetization dynamics as compared to systems with smaller point-contact diameter D_c and high external fields H_{ext}. In particular, both the larger D_c value and the smaller strength of H_{ext} should allow for more complicated magnetization configurations, leading to an even richer set of nonlinear localized modes than that reported in Refs. 21, 22, and 25. For this reason and keeping in mind a comparison with the experiments performed in Ref. 14, we have chosen the value $D_c=80$ nm for the contact diameter and $H_{ext}=30$ Oe for all result sets presented below.

This relatively large value of D_c allowed us to choose larger lateral mesh size than in Ref. 22: in this study we use

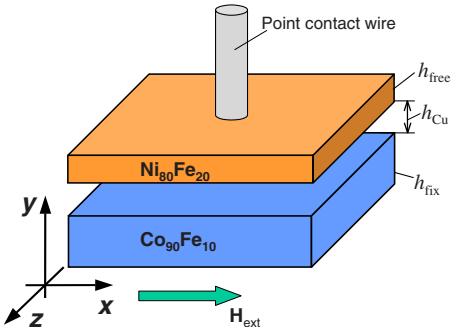

FIG. 1. (Color online) Geometry of the complete trilayer system. To study the magnetization dynamics, periodic boundary conditions are applied to the magnetization configuration in x and z directions

the in-plane cell size 5×5 nm^2. In order to understand the influence of the interlayer interaction on the SPC-induced dynamics, we have studied both a *single-layer* system and the *complete magnetic trilayer* consisting of materials as used in Ref. 14. Geometry of the complete (trilayer) system is shown in Fig. 1; a single-layer system studied here is obtained from the system shown in Fig. 1 by removing the lower (CoFe) layer. For the single-layer system the layer thickness $h_{free}=5$ nm and magnetic parameters corresponding to $Ni_{80}Fe_{20}$ (permalloy) were used: saturation magnetization $M_S=640$ G, exchange stiffness constant $A=1\times10^{-6}$ erg/cm, cubic magnetocrystalline anisotropy with $K_{cub}=5\times10^3$ erg/cm^3. For the trilayer system we have adopted the parameters of the "fixed" (hard) layer as for $Co_{90}Fe_{10}$, namely $M_S=1500$ G,[28] $A=2\cdot10^{-6}$ erg/cm [various sources give the values of the CoFe exchange stiffness in the range $A=(1-3)\cdot10^{-6}$ erg/cm], the layer thickness $h_{fix}=20$ nm and the spacer thickness (distance between two magnetic layers) $h_{Cu}=4$ nm.[14] Both magnetic layers were not discretized further into sublayers. It was checked that such a discretization, leading to a large increase in the computational time, did not significantly affect the results.

In order to avoid the artificial influence of the system borders, we have used periodic boundary conditions (PBCs). To suppress the spin-wave propagation between different PBC replica, we employ the damping parameter, which increased toward the simulated area borders as described in Refs. 22 and 23. The spatial dependence of the damping coefficient in the form $\lambda(r)=\lambda_0+\Delta\lambda\cdot[1+\tanh((r-R_0)/R_{dec})]$ was employed (r denotes the distance to the point-contact center) with $\lambda_0=0.02$ being the "native" material damping constant, $R_0=1000$ nm, $R_{dec}=100$ nm, and the increase parameter $\Delta\lambda=1.0$. For the lateral size of the simulated area $L\times L=2000\times2000$ nm^2 this damping profile is sufficient to fully suppress the artificial spin-wave interference arising due to PBC. We note that the increased damping near the borders would suppress the reflected spin waves also for open (fixed or free) boundary conditions (OBCs). However, periodic boundary conditions have another two advantages compared to OBC. First, for PBC there is no stray field caused by open borders so that the magnetization configuration is not disturbed by this field. Second, there is no need to use the zero-padding technique along each spatial dimension

required for OBC by calculating the stray field via the fast Fourier transformation technique. Due to this zero padding the total system size for OBC on a two-dimensional (2D) grid is four times larger than for PBC.

We have also studied the influence of the Oersted field of the *dc*-current (see Sec. III B). Because the current distribution in the experimental setup is not known exactly, we could not compute the Oersted field directly from this distribution. For this reason, we adopted another strategy to study the Oersted field effect, which is explained at the beginning of Sec. III B.

The magnetization dynamics itself was simulated using our commercially available micromagnetic package MICROMAGUS (Ref. 29) with the extensions allowing to use (i) the site-dependent damping constant as explained above and (ii) the site-dependent current density in order to mimic the current flowing through the point-contact area only. Thermal fluctuations were neglected ($T=0$). Spin torque acting on the *free layer only* was included by adding the Slonczewski torque term $\Gamma_{st}=a_J[\mathbf{M}\times[\mathbf{M}\times\mathbf{p}]]$ to the "normal" Landau-Lifshitz-Gilbert (LLG) equation. The amplitude of this torque a_J is proportional to current strength I and its spin-polarization degree P and depends also on the magnetic layer thickness h, the contact area $S_c=\pi R_c^2$, and magnetization M_S (see, e.g., Ref. 30),

$$a_J=\frac{\hbar\cdot I\cdot P}{2|e|M_S^2\cdot h\cdot S_c}. \tag{1}$$

The spin-polarization direction of electrons $\mathbf{p}$ in the *dc*-current flowing through the contact area was chosen to be *opposite* to the applied field direction $\mathbf{H}_{ext}$ for a *single-layer* system and *opposite* to the *local instantaneous magnetization direction* of the fixed layer for a *trilayer* system. The reason for this choice is the following: the magnetization of a free layer in real experiments is supposed to be excited by spin-polarized electrons *reflected* from the fixed magnetic layer (of a trilayer system) toward the free one. This corresponds to the case when the conducting electrons of the dc current flow from the free toward the fixed layer; for this current direction the current I in Eq. (1) is assumed to be positive.

III. RESULTS AND DISCUSSION

A. Magnetization dynamics of the single-layer system in the absence of the Oersted field

In order to understand the influence of various physical factors on the magnetization dynamics separately, we proceed by "switching on" these factors in turn, thus isolating corresponding effects. Hence we start our study with the simplest system including the free layer only and neglecting the Oersted field of the dc current.

Oscillation power spectra for this system (Py layer with the thickness $h_{Py}=5$ nm, point-contact diameter $D_c=80$ nm, in-plane field $H_{ext}=30$ Oe) are shown in Fig. 2. This figure displays the oscillation power spectra of the m_z magnetization component, which is the in-plane component perpendicular to $\mathbf{H}_{ext}$ (see Fig. 1 for the system geometry).

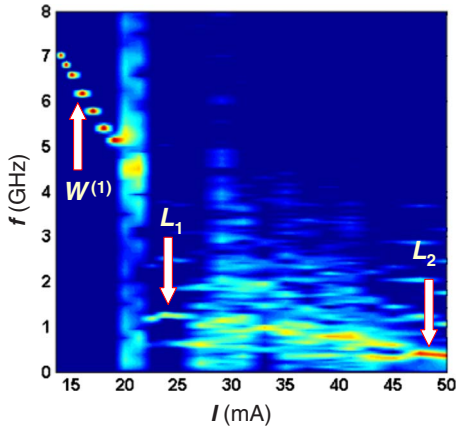

FIG. 2. (Color online) Spectral power of the m_z component (in-plane component perpendicular to the external field) as the function of the current strength in the single-layer system without the Oersted field. Arrows indicate the position of modes analyzed below in more detail (see Figs. 3–5) The discrete character of the $f(I)$ dependence of the W_1 mode is an image artifact due to the discrete set of simulated currents and rapid frequency decrease with current for this mode.

1. Propagating wave mode

The first mode observed after the oscillation onset is the propagating wave mode W_1 (Slonczewski mode) predicted already in Ref. 18. The index in the notation W_1 is necessary to distinguish W-mode in this simplest system from propagating wave modes in other systems studied below. The W_1 mode exists in the relatively broad current range ($I_W\approx 14-20$ mA) and its frequency decreases *continuously* with growing current (the discrete character of the $f(I)$ dependence for this mode seen in Fig. 2 is an image artifact arising due to the discrete set of currents used in simulations and rapid frequency decrease with current).

The threshold current value for the oscillations onset is $I_{th}\approx 14$ mA and the corresponding frequency is $f_{th}\approx 7.05$ GHz. It is instructive to compare these values to analytical calculations for the W mode.[18,20] We recall that these calculations predict the threshold current

$$\sigma I_{th}\approx\frac{1.86\cdot D(H_0)}{R_c^2}+\Gamma(H_0), \tag{2}$$

where the factor $\sigma=g\mu_B P/(2|e|M_S\cdot h\cdot S_c)$ (Ref. 20) is related to our spin torque amplitude a_J via $\sigma I=\gamma M_S\cdot a_J$. The first term in Eq. (2) describes the (dominant) energy loss due to the spin-wave emission by the point-contact area and is proportional to the spin-wave dispersion $D(H_0)$. For the field-in-plane geometry this dispersion reads as

$$D(H_0)=\frac{2\gamma A}{M_S}\cdot\frac{H_0+2\pi M_S}{\sqrt{H_0(H_0+4\pi M_S)}}. \tag{3}$$

The second term in Eq. (2) $\Gamma(H_0)=\gamma\lambda\cdot(H_0+2\pi M_S)$ describes the energy losses within the point-contact area due to the Gilbert damping. In our case these losses are negligibly small.

For the system geometry ($h=5$ nm, $R_c=40$ nm), material parameters ($M_S=640$ G, $A=1\cdot10^{-6}$ erg/cm, and $\lambda=0.02$), current polarization $P=0.4$, and external field $H_0=30$ Oe used in our simulations, the analytically calculated threshold current is $I_{th}^{an}\approx37$ mA. This result is about 2.5 times larger than the simulated value ($I_{th}^{sim}\approx14$ mA).

Analytical formula for the oscillation frequency[31] $\omega_{th}^{an}=\omega_0+Dk_0^2$ contains the homogeneous FMR frequency for the in-plane field $\omega_0=\sqrt{H_0(H_0+4\pi M_S)}$, and the wave vector of the excited circular spin wave, which was found to be[18,20] $k_0=1.2/R_c$. In contrast to the large discrepancy for the threshold currents, the frequency calculated analytically using this expression $f_{th}^{an}=\omega_{th}^{an}/2\pi\approx7.85$ GHz is only slightly above the frequency $f_{th}^{sim}=7.05$ GHz obtained numerically.

A possible reason for the large disagreement between the analytically predicted and numerically simulated threshold currents could be the approximations made by the derivation of Eq. (2) for I_{th}^{an}: first, it was obtained for the *perpendicularly* magnetized point contact, and second, it was assumed that the group velocity of emitted spin waves is *isotropic* with respect to the propagation direction. The partial adjustment of Eq. (2) to our case of an in-plane magnetized contact could be achieved by using expression (3) for the spin-wave dispersion in case of an *in-plane* magnetization. However, the dependence of the spin-wave velocity on the propagation direction could not be taken into account. In our case the point-contact diameter is relatively large, so that the wave vectors of the emitted waves $k\sim1/R_c$ are relatively small. Hence the wave group velocity substantially depends on the angle between the wave propagation direction and external field (see grayscale maps in Fig. 3). This high anisotropy of the group velocity could lead to significant discrepancies between analytical calculations and numerical data.

At the same time the expression for the threshold frequency $\omega_{th}^{an}=\omega_0+Dk_0^2$ uses—besides the in-plane spin-wave dispersion factor D—only the wave vector $k_0\sim1/R_c$, which exact value relies mainly on the geometrical consideration (circular shape of the current-flooded area). Hence the analytical prediction for the oscillation frequency should be more reliable, leading to a much better agreement between theory and simulations, as found above.

These arguments are supported, in particular, by analogous comparisons for the nanocontact with a smaller diameter ($D_c=40$ nm) in Refs. 21 and 22, where the anisotropy of the group velocity was much lower due to larger wave vectors. The agreement between analytical and numerical threshold currents for this case was, indeed, significantly better (see Refs. 21 and 22 for details).

With increasing current the frequency decreases from its initial value $f_{th}\approx7$ GHz at $I_{th}\approx14$ mA to $f\approx5$ GHz at $I\approx20$ mA, where the transition to localized modes occurs (see below). This (in our case nearly linear) frequency decrease due to the growing oscillation amplitude is a nonlinear effect which is well understood theoretically[20,32] and hence will not be further discussed here.

Concluding this discussion of the propagating wave mode, we would like to emphasize the modulation of the main wave profile by a "secondary" wave with the vector $k\approx2k_0$ approximately twice as large as the "main" wave vector k_0. This modulation, clearly seen at grayscale maps in Fig. 3, is due to another nonlinear effect arising due to the conservation of the local-moment magnitude: $M_x^2+M_y^2+M_z^2=M_S^2$. This condition leads to the contribution of the spin wave with the frequency corresponding to M_x oscillations to the wave pattern of the M_z projection. The effect becomes more pronounced with the increase in the magnetization oscillation amplitude; the picture shown in Fig. 3 corresponds to $I=16$ mA, where the oscillation amplitude of the M_z projection under the point contact is close to its maximal value $m_z^{max}=M_z^{max}/M_S\approx1$.

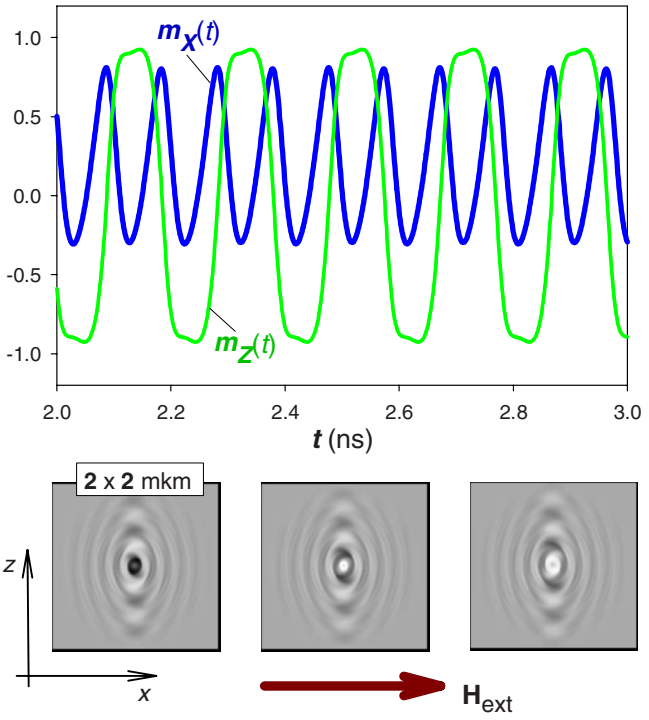

FIG. 3. (Color online) Magnetization time dependencies and snapshots of the magnetization configurations as grayscale images of the m_z component for the propagating mode W_1 in the single-layer system. The Oersted field is neglected. Coordinate axis and the external field direction ($H_{Oe}=30$ Oe) are the same for all grayscale images shown on subsequent figures.

2. Localized modes

When the current strength exceeds the next critical value $I_{th}^{loc}\approx20$ mA, a large frequency jump down to $f\approx1.2$ GHz occurs. This frequency is well below the homogeneous FMR frequency $f_0=(\gamma/2\pi)\sqrt{H_0(H_0+4\pi M_S)}\approx1.4$ GHz for the film studied here so that magnetization oscillations after the jump (above I_{th}^{loc}) should correspond to a localized mode. The spatiotemporal analysis of magnetization configurations reveals that all modes occurring for $I>I_{th}^{loc}$ are indeed localized. Dynamical processes responsible for observed magnetization oscillations (see figures below) are qualitatively different for various modes. In many cases these processes are also highly irregular, so we describe and discuss below only those localized modes, which correspond to relatively simple magnetization dynamics.

Magnetization oscillations for the first such mode, which appears just after the transition from the propagating wave

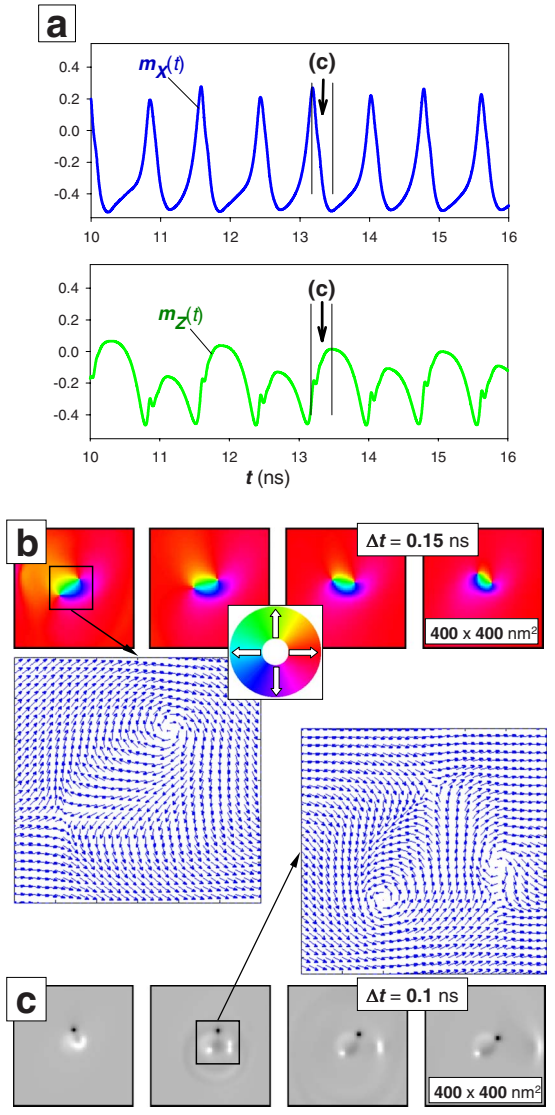

FIG. 4. (Color online) Magnetization time dependencies (a) and snapshots of the magnetization configurations (b) and (c) for the first localized mode L_1 in the single-layer system for $\mathbf{H}_{Oe}=0$. Panel (b) shows the rotation process of the main vortex-antivortex pair (images of the in-plane magnetization orientations) together with the arrow plot of a typical V-AV configuration. Panel (c) illustrates the creation, propagation and decay of a satellite V-AV pair (gray-scale images of the out-of-plane magnetization orientations m_y).

mode W_1 to localized oscillations, are shown in Fig. 4. This first localized mode (L_1-mode) has a completely different nature compared to the spin-wave "bullet" observed in systems with the relatively small point-contact diameter (D_c =40 nm).[20–23] The abovementioned "bullet" mode has a relatively homogenous core structure, whereby the magnetization oscillation amplitude decreases exponentially with the distance from the contact center. In contrast to the "bullet" mode, in our system the magnetization structure of the first localized mode is highly inhomogeneous: magnetization oscillations are caused by an appearance and rotation of a vortex-antivortex pair. This qualitative difference between the two systems studied here and in Refs. 20–22 is due to the small contact diameter D_c=40 nm and the large external field H_{ext}=2 kOe used in the papers cited above: both these factors strongly favor a homogeneous magnetization configuration of the localized mode core found in Refs. 20–23. In our case, where the point-contact diameter is twice as large and the external field is nearly absent (H_{ext}=30 Oe), a formation of more complicated excitations—vortex-antivortex (V-AV) pairs—becomes possible.

As it can be seen from Fig. 4, two major processes contribute to the dynamics of the L_1 mode in our system: (i) rotation of a V-AV pair with a relatively large V-AV distance [Fig. 4(b)] and (ii) generation and subsequent translational motion of a much smaller V-AV [Fig. 4(c)].

To start the analysis of these two processes, we first point out that due to the periodic boundary conditions applied to the system and the homogeneous starting magnetization state, magnetic excitations with nonzero vorticity should appear in pairs in order to guarantee the conservation of the total topological charge.[33,34] This situation is qualitatively different from those observed for small patterned nanoelements, where due to open boundaries and the out-of-plane external field the formation of a *single* vortex was possible.[25]

Both rotational and translational motions of a V-AV pair mentioned above have been studied by Komineas and Papanicolaou.[34,35] They showed that a V-AV pair should *rotate* when vortex and antivortex have *opposite* polarities and undergo a *translational* motion when the polarities of a vortex and antivortex are the *same*. Results of our simulations agree with this analytical statement: as it can be seen from the grayscale maps in Fig. 4(c), polarities of vortex and antivortex are *opposite* for the large *rotating* V-AV pair, but their polarities *coincide* within the small *translationally* moving V-AV pair.

The next step is obviously the quantitative comparison of the rotation frequency and the translational velocity of a V-AV pair predicted in Refs. 34 and 35 with our simulation results. In Ref. 34 it was shown that a V-AV pair with vortex and antivortex having opposite polarities possesses a zero linear momentum (so that the pair center does not move) but a nonzero *angular* momentum $\mathbf{L}$ so that such a pair should rotate ($\mathbf{L}$ increases as $\sim d^2$ with the V-AV separation distance d). The angular velocity of this rotation $\boldsymbol{\omega}$ can be determined from the condition that for this velocity the extended energy functional $F=E-\boldsymbol{\omega}\mathbf{L}$ in the rotating coordinate system should possess a stationary point. The total magnetic energy of a V-AV pair in this functional $E=E_{ex}+E_{an}$ consists—in the approximations used in Ref. 34 (no external field, large V-AV separation)—from the sum of exchange E_{ex} and the anisotropy E_{an} energies of the vortex and antivortex. In the notation of Komineas E_{an} includes also the demagnetizing energy in the thin-film geometry.

The form of the extended energy functional F together with the scaling arguments similar to those used in the nonlinear dynamics of continuous media enables the determination of the rotation frequency f of the V-AV dipole. The explanation given in the PRL-paper[34] was necessarily very brief; in addition, scaling arguments used in Ref. 34 are not commonly familiar to the micromagnetic community, so we present the basic line of these arguments here in order to make our paper self-contained. The main idea is that the stationary point of the extended energy functional $F=E$

$-\boldsymbol{\omega}\mathbf{L}$ should "survive" the rescaling of spatial variables, which by itself does not change the physics of the system. In 2D systems (thin-film limit) the exchange energy E_{ex} is invariant with respect to such a rescaling, because E_{ex} is a 2D integral over a *square* of the magnetization *gradient*. In contrast, E_{an} is not invariant with respect to this transformation, being in the simplest case a 2D integral over the second power of the magnetization components themselves. Hence the energy functional $F=E-\boldsymbol{\omega}\mathbf{L}=E_{ex}+E_{an}-\boldsymbol{\omega}\mathbf{L}$ may have a stationary point which is stable with respect to rescaling only when $E_{an}-\boldsymbol{\omega}\mathbf{L}=0$. Using this relation together with the expressions for the vortex anisotropy energy E_{an} and the dependence of the angular momentum $\mathbf{L}$ on the V-AV separation d, Komineas[34] derived the rotation frequency for the V-AV pair, which in nonreduced units reads as

$$f=\frac{2}{\pi}\cdot\frac{\gamma A}{M_S d^2}, \tag{4}$$

where γ is the gyromagnetic ratio.

Application of this expression to our case requires some care: the V-AV distance changes noticeably during the pair rotation, so that one should substitute into Eq. (4) the inverse square distance averaged over the rotation period, which for our simulation conditions was found to be $\langle 1/d^2\rangle = 2.07\cdot 10^{-4}$ nm^{-2}. With magnetic parameters used here ($M_S=640$ G and $A=1\cdot 10^{-6}$ erg/cm), we obtain the analytical value for the rotation frequency $f_{rot}^{an}\approx 0.37$ GHz.

The calculation of the f_{rot} from the simulated data is a nontrivial task because the continuous rotation of the V-AV pair is only one of two dynamical processes observed during magnetization oscillation period. The second process—creation of the satellite V-AV pair—leads to a significant "jump" of the vortex belonging to the main pair. This nearly instantaneous vortex displacement can obviously not be described by the theory of Komineas. Hence by the evaluation of the simulated rotation frequency only the part of the V-AV orbit corresponding to the continuous V-AV rotation should be taken into account. The rotation frequency determined this way is $f_{rot}^{sim}\approx 0.44$ GHz.

The agreement between simulations and analytical theory can be considered as satisfactory, taking into account that neither the V-AV magnetodipolar interaction, nor the spin torque acting on both vortex and antivortex are taken onto account by derivation of estimation (4). The most significant correction probably comes from the spin torque acting on the *antivortex*, because this torque changes its value and direction when the antivortex moves around the center of the point-contact area. We also note that the V-AV exchange interaction can be safely neglected, because the V-AV separation d in this case is much larger than the exchange length $l_{ex}=(A/2\pi M_S^2)\approx 6.23$ nm.

Now we turn our attention to the second type of the V-AV pair dynamics—translational motion, also observed for the first localized mode L_1. Figure 4(c) demonstrates that during the rotation of the main (large) V-AV pair another (much smaller) V-AV pair consisting of a vortex and antivortex with *the same* polarities is generated. Such a composite object has zero angular momentum (so that such a pair does not rotate)[35] but a *nonzero* linear momentum $\mathbf{P}$, which results in a *translational* motion of this V-AV pair (the so-called Kelvin motion, well known from the fluid dynamics). This translational motion can be clearly seen in Fig. 4(c) and its velocity can be compared to the analytical result from Ref. 35.

Analytical estimation made in Ref. 35 is based for the translational V-AV motion on the extended energy functional $F=E-\boldsymbol{v}\mathbf{P}$ in a translationally moving coordinate system, where $\boldsymbol{v}$ is the linear velocity of the V-AV pair. The same scaling arguments concerning the stability of the stationary point of this functional with respect to the rescaling of spatial variables apply to this case also. Together with the expression of the anisotropy energy for the V-AV pair these arguments lead to the following estimation for the pair velocity in the limit of large V-AV separations:

$$f=\frac{2\gamma A}{M_S d}. \tag{5}$$

Substituting the same material parameter values and the V-AV separation $d\approx 25$ nm determined from the simulated magnetization configuration shown in Fig. 4(c) into Eq. (5), we obtain the analytical estimation $v^{an}\sim 2.2\cdot 10^4$ cm/s. The pair velocity for this system, measured from simulated magnetization configurations, is $v^{sim}\approx 6.3\cdot 10^4$ cm/s. The large difference between these velocity values is most probably due to the small V-AV distance (here d is only about several exchange lengths $l_{ex}\approx 6$ nm). For closely placed vortex and antivortex, their strong exchange and magnetodipolar interactions can lead to significant deformation of their structures.

An important circumstance is that this V-AV pair is gradually destroyed during its translational motion due to the presence of the finite-energy dissipation, which could not be taken into account by the analytical theory.[35] This gradual decay is in contrast to the steady-state rotation of the large V-AV pair with the opposite V-AV polarities, which is due to the constant energy supply via the spin-polarized current. We also note that the formation and emission of this small V-AV pair is an important mechanism of the magnetic energy irradiation out of the point-contact area.

When the current is increased further ($I>26$ mA, see Fig. 2), a variety of more complicated and partially irregular localized modes appear. The overall trend is the increase in the number of V-AV pairs generated and annihilated per unit time. We postpone the detailed discussion of the intriguing magnetization dynamics in this current region to future publications and discuss only the regular localized mode L_2, observed for high-current values (40–50 mA).

Such a strong current leads to the periodical creation/annihilation of a vortex-antivortex *quadrupole*, consisting of two vortices and two antivortices all having the same polarity (Fig. 5), and located symmetrically with respect to the point-contact center. The formation of this V-AV quadrupole starts with the appearance of a ring-shaped magnetization structure [see the first grayscale map in Fig. 5(b)], which evolves very fast into two V-AV pairs which form a nearly symmetrical V-AV quadrupole. From the point of view of nonlinear excitation dynamics such a quadrupole represents the next possible stable excitation kind (after a single V-AV

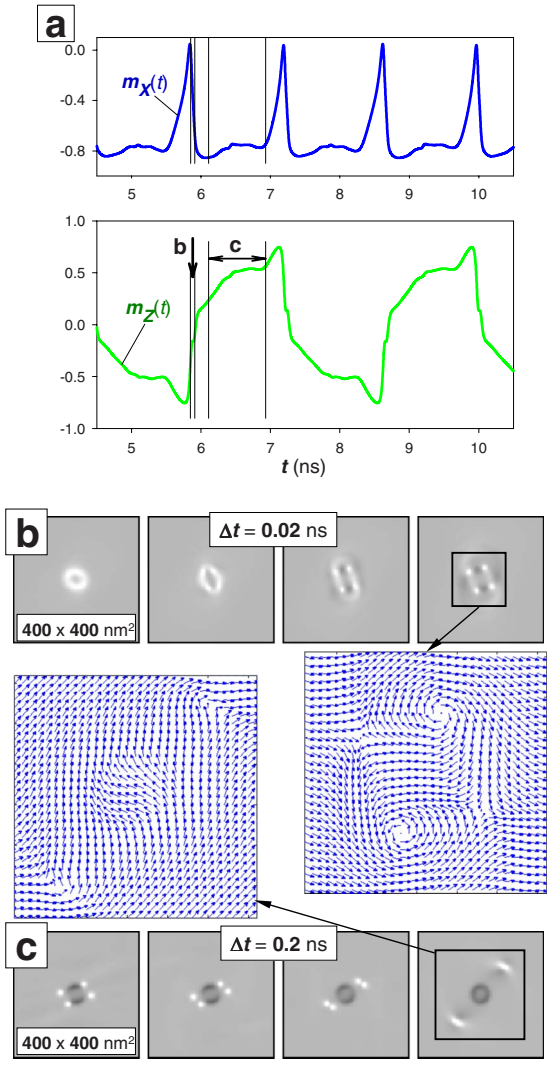

FIG. 5. (Color online) Magnetization time dependencies (a) and grayscale snapshots (b) and (c) of the out-of-plane magnetization component m_y for the second localized mode L_2 (single layer, $\mathbf{H}_{\mathrm{Oe}}=0$). Panel (b) shows the creation process of two V-AV pairs and an in-plane arrow plot of a typical V-AV quadrupole configuration. Panel (c) displays the propagation and decay of the two V-AV pairs. Time intervals corresponding to the image rows of (b) and (c) are marked with vertical lines on $m_z(t)$ plot in the panel (a).

pairs) for systems where the total topological charge is initially zero and should be conserved. The whole process of the quadrupole formation shown in detail in Fig. 5(b) is very fast, taking only ~50 ps.

The quadrupole built this way does not rotate (because, as mentioned earlier, all its vortices and antivortices have the same polarity), so it can disappear only relatively slowly via the symmetry breaking with respect to the V-AV distances and Kelvin motion of the V-AV pairs arising after this symmetry breaking. The lifetime of the V-AV quadrupole limited by this process is ~1 ns as it can be seen from the magnetization time dependencies [Fig. 5(a)] and grayscale maps of the out-of-plane magnetization projections [Fig. 5(c)]. The two solitons, each representing one V-AV pair, propagate in opposite directions and decay due to the "normal" energy damping. These solitons are responsible for the energy emission out of the point-contact area for this localized mode.

We note once more that in all cases considered above the oscillation frequency of the m_x component is two times larger than that of the m_z component, as it can be clearly seen from Figs. 3(a), 4(a), and 5(a). This means that by experimental observations of these modes using the GMR effect, the strong second harmonics should be present not only due to the nonsinusoidal character of m_z-oscillations but also due to the mixing of signals from m_x and m_z components. This mixing unavoidably happens when the magnetization of the fixed layer deviates (even slightly) from the external field direction, e.g., due to the influence of a random magnetocrystalline anisotropy of this fixed layer. As mentioned above, for $Co_{90}Fe_{10}$ often used in such experiments,[12,14] the cubic anisotropy constant $K_{\mathrm{cub}}=-5.6\cdot10^5$ erg/cm^3 is not small,[28] so that even in nanocrystalline materials noticeable deviations of the magnetization from its average direction (along the external field) can be expected.

B. Magnetization dynamics for the single-layer system: influence of the Oersted field

In this subsection we discuss the influence of the Oersted field, induced by the spin-polarized *dc*-current, on the magnetization dynamics. When a quantitative comparison with real experiments made on relatively large point contacts and in small external fields is planned, one cannot neglect the influence of the Oersted field, because for this situation it is not small compared to the external field. Hence the corresponding influence can crucially change the magnetization dynamics, especially taking into account that the Oersted field of a thin wire is strongly inhomogeneous.

Unfortunately, it is not possible to compute this field quantitatively, because the experimental setup and the current distribution in contact leads are not known exactly. For this reason we have adopted the following strategy to study the Oersted field effect. We are interested in the Oersted field acting on the free layer directly under the point contact and near it. The Oersted field in this area is created mainly by the current flowing through (i) the point-contact wire itself and (ii) the lead regions attached to the contact. The current distribution inside a contact wire with a circular cross section possesses the cylindrical symmetry relative to the wire axis. Further, the contact diameter is usually much smaller than the lateral lead size. So in a good approximation, the current flow within the above mentioned lead regions is similar to the water stream flowing from the large basin into a narrow drain channel and hence possesses the same cylindrical symmetry.

The above arguments, which have been presented and quantitatively elaborated by Miltat,[36] lead to the conclusion that the Oersted field in the region of interest has the circular symmetry (field lines are circular with the centers lying on the contact wire axis). The field magnitude can then be calculated using the same argument as by computing the field of an infinite straight wire from Maxwell equations: the field circulation along the given circle is proportional to the total current flowing inside this circle. Because in a real experi-

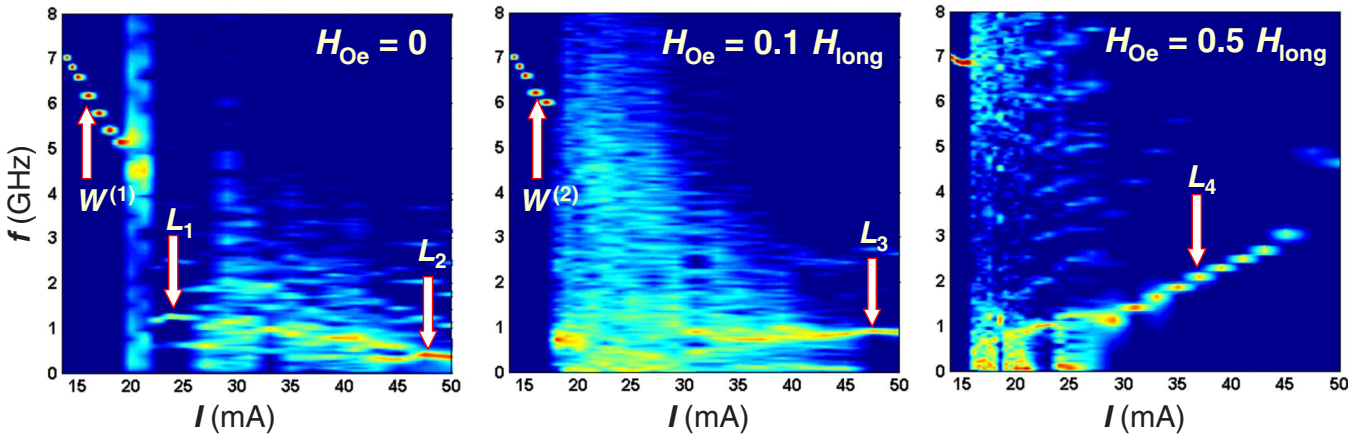

FIG. 6. (Color online) Spectral power of the m_z component vs current strength in the single-layer system for different strengths of the Oersted field computed as explained in the text. Arrows show the positions of modes analyzed in detail below. The discrete character of the $f(I)$ dependence for the W_1, W_2, and L_4 modes is an image artifact (see caption to Fig. 2).

ment we deal with a complicated multilayer system consisting of layers with different conductivity (in particular, with Cu/Au layers on the top of the "free" magnetic layer[12]), it is not known, which fraction of the total current injected into the contact wire, flows inside the circle of the given radius within the "free" (Py) magnetic layer. So, in order to study the Oersted field effect, we proceed in the following way. First we calculate the field $\mathbf{H}_{\text{inf}}(I,r)$ generated by a current I in an *infinitely long* wire with the diameter of the point contact (r is the distance from the contact center). Then we assume that the actual Oersted field has the same circular symmetry, but is weaker than $\mathbf{H}_{\text{inf}}(I,r)$. To account for this weakening, we introduce the coefficient κ ($0 \leq \kappa \leq 1$), compute the Oersted field as $\mathbf{H}_{\text{Oe}}(I,r) = \kappa \cdot \mathbf{H}_{\text{inf}}(I,r)$ and study magnetization dynamics for various values of κ.

Results of these studies are summarized in Fig. 6, where the oscillation power maps in the current-frequency plane in presence of $\mathbf{H}_{\text{Oe}}$ (middle and right panels) are shown together with the case when $\mathbf{H}_{\text{Oe}}$ is absent (left panel, the same as in Fig. 2). These oscillation power plots allow to identify the following qualitative effects of the Oersted field on the magnetization dynamics:

(i) "on average," the oscillation spectra become more regular, especially for large Oersted fields [see Fig. 6(c), $\kappa = 0.5$], where well-defined spectra with sharp peaks for nearly all current values are observed. This effect is due to the stabilizing influence of the Oersted field, which—at least for large κ-values—is strong enough to guarantee the existence of well-defined modes, preventing the system from sliding into a quasichaotic behavior.

(ii) The current region, where the propagating wave mode exists, narrows with increasing κ This contraction can be explained by a strongly nonhomogeneous character of the Oersted field in the geometry under study, which induce a nonhomogeneous and asymmetrical equilibrium magnetization configuration (in the absence of SPC-induced oscillations). Such a configuration obviously suppresses the oscillation mode represented by the wave propagating circularly out of the point-contact area.

(iii) Localized modes containing V-AV pairs also behaves qualitatively different in presence of the Oersted field, because this circular field acts differently on a vortex and an antivortex, thus disturbing a free rotation of a V-AV pair (see discussion below).

To study the magnetization dynamics in presence of the Oersted field in more detail, we consider first the case of the weak field $\mathbf{H}_{\text{Oe}} = 0.1 \cdot \mathbf{H}_{\text{inf}}$. For small currents we observe again the propagating mode W_2 similar to that found in the absence of $\mathbf{H}_{\text{Oe}}$. As explained above, the current region where this mode exists is narrower than for W_1 ($\Delta I_{W2} = 15-17.5$ mA for $\kappa = 0.1$ instead of $\Delta I_{W1} = 15-20$ mA for $\mathbf{H}_{\text{Oe}} = 0$). Due to the abovementioned asymmetry of the underlying equilibrium magnetization state caused by the Oersted field (and also due the overlapping of the Oersted field with the homogeneous external field $\mathbf{H}_0 = 30$ Oe used in all our simulations presented here), the group velocity of a spin wave significantly depends on the propagation direction. Hence magnetization pattern for the W_2-mode becomes circularly asymmetric (see grayscale maps in Fig. 7).

By higher currents the propagating wave mode vanishes, and the localized modes appear. In presence of the Oersted field these modes differ qualitatively from localized modes when $\mathbf{H}_{\text{Oe}}$ is neglected. In particular, it is instructive to compare the localized mode L_2 arising at the high current $I = 48$ mA at $\mathbf{H}_{\text{Oe}} = 0$ (see Fig. 5) with the localized mode L_3 appearing for the same current, but for $\mathbf{H}_{\text{Oe}} = 0.1 \cdot \mathbf{H}_{\text{inf}}$ (shown in Fig. 8). From grayscale maps and arrow plots shown in Fig. 8 it is clear that in contrast to the quadrupole V-AV mode in the absence of $\mathbf{H}_{\text{Oe}}$, the magnetization configuration of the L_3 mode at higher currents even in presence of a relatively weak Oersted field ($\kappa = 0.1$) contains most of the time only a single V-AV pair. This fact can be again attributed to the strong circular asymmetry of the magnetization state in presence of $\mathbf{H}_{\text{Oe}}$, so that the formation of a highly symmetric V-AV quadrupole becomes impossible.

Magnetization dynamics of this new L_3 mode is also completely different. Due to the same reason—circularly asymmetric equilibrium magnetization configuration—the V-AV pair cannot rotate free around its center even when vortex and antivortex have opposite polarities. Magnetization dynamics of the L_3-mode is thus governed by the *oscillation of the vortex position*, whereby the antivortex remains nearly

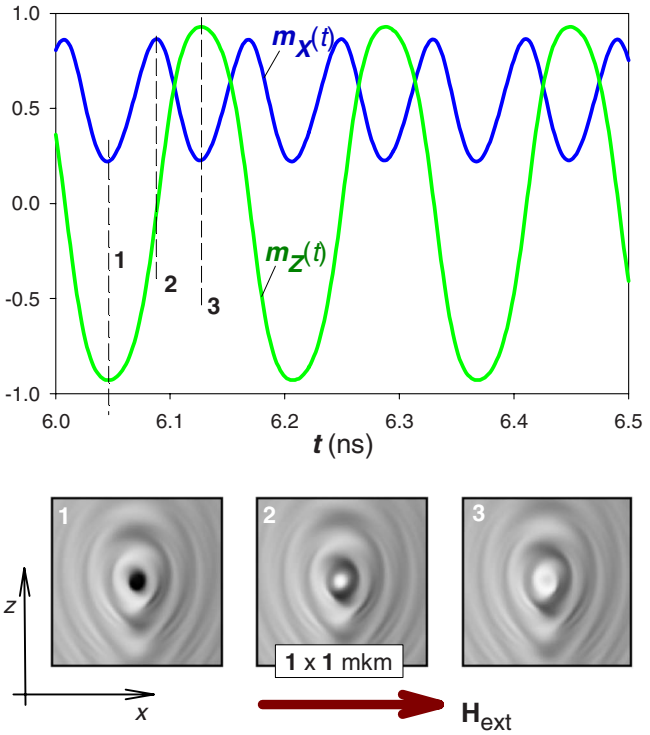

FIG. 7. (Color online) The same as in Fig. 3 for the propagating mode in the single-layer system for $\mathbf{H}_{\mathrm{Oe}}=0.1\mathbf{H}_{\mathrm{inf}}$.

immobile. During these oscillations the vortex generates a second V-AV pair with a very small V-AV distance and the same polarities, which are, however, *opposite* to the polarity

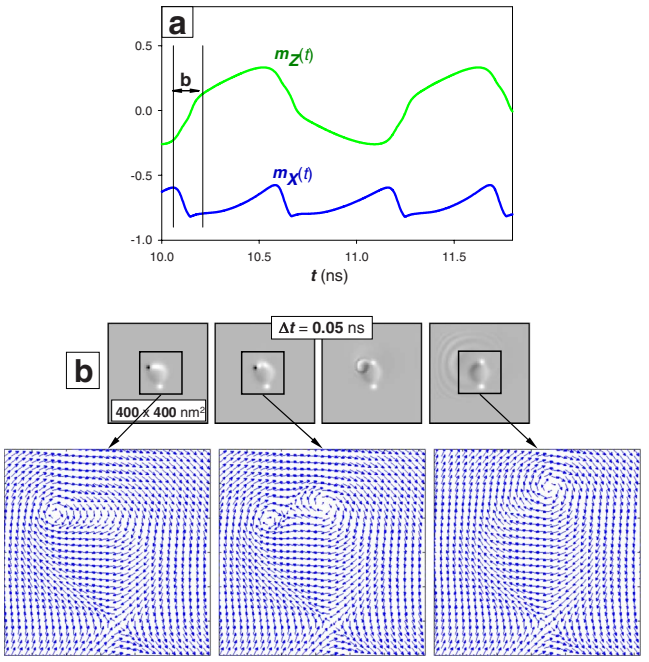

FIG. 8. (Color online) (a) Magnetization time dependencies for the high-current localized mode L_3 in the single-layer system for $\mathbf{H}_{\mathrm{Oe}}=0.1\mathbf{H}_{\mathrm{inf}}$. (b) Oscillations of the main V-AV pair, accompanied by the creation and annihilation of a satellite V-AV pair (snapshots of the out-of-plane magnetization component m_y and in-plane arrow plots).

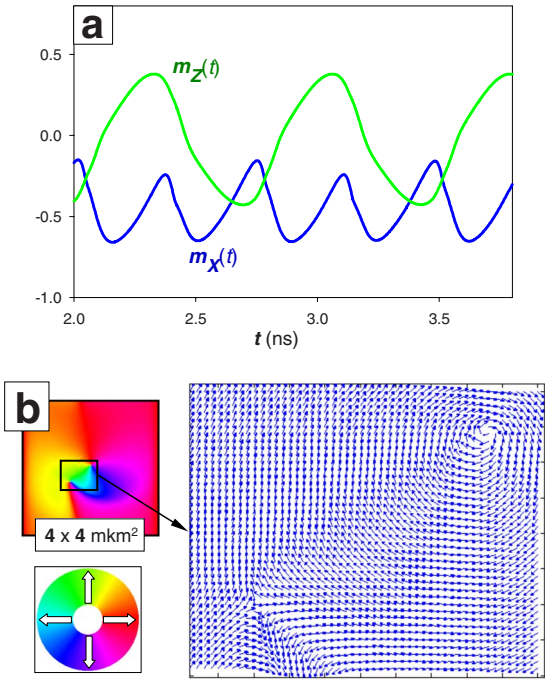

FIG. 9. (Color online) (a) Magnetization time dependencies for the high-current localized mode L_4 in the single-layer system for the large Oersted field $\mathbf{H}_{\mathrm{Oe}}=0.5\mathbf{H}_{\mathrm{inf}}$; (b) Image of the in-plane magnetization orientation for the whole simulation area and the enlarged in-plane arrow plot of the V-AV pair.

of the *initial* vortex. The antivortex from this new small V-AV pair annihilates with the initial vortex (radiating a burst of spin waves), thus leaving a single vortex with the polarity opposite to the initial vortex, so that effectively the polarity of the vortex in the initial large V-AV pair is reversed. Then this new vortex starts to move in the opposite direction, generates a new small V-AV pair and the process in repeated. A very similar process was reported as a mechanism to change the vortex polarity during a motion of a single vortex in Ref. 37.

When the Oersted field coefficient κ is increased further, the propagating mode region contracts even more (right panel in Fig. 6 with $H_{\mathrm{Oe}}=0.5\cdot H_{\mathrm{inf}}$). Increasing the current for this κ value, we still observe after a W-mode a relatively narrow region of irregular dynamics, after which a transition to a localized mode L_4 similar to that shown in Fig. 8 takes place. Due to the larger Oersted field and stronger deformation of the magnetization configuration the (also immobile) antivortex of this L_4 mode is located farther from the point-contact center than for the L_3-mode at the same current [Fig. 9(b)]. Magnetization dynamics of the L_4 mode is governed by the same process of the vortex oscillation accompanied by the creation annihilation of a small V-AV pair as for the L_3 mode. An important point is that the large Oersted field leads for this case to a strong (and approximately linear) increase in the mode frequency with the current strength because the oscillation frequency of the vortex in the potential well created by the Oersted field near the point-contact center increases with the current strength.

Concluding this subsection, we note that the Oersted field can be made different for *the same current strength* (at least

up to some extent) by changing the electric setup. This offers a possibility to control the dominating oscillation mode of the point-contact device by adjusting the geometry of the contact wires, if the corresponding Oersted field changes could be achieved by such an adjustment.

C. Magnetization dynamics for the CoFe/Cu/Py trilayer system: Influence of the "hard" magnetic layer

The next important question for the SPC-induced magnetization dynamics is the influence of the "fixed" magnetic layer on magnetization oscillations of the "free" layer. Up to our knowledge, this influence was not studied yet for the point-contact setup in the extended thin-film geometry, so the results presented below are especially interesting. We recall that the 'fixed' layer parameters have been chosen to imitate the $Co_{90}Fe_{10}$ underlayer used in the system studied experimentally in Ref. 14: $M_S=1500$ G, $A=2\cdot10^{-6}$ erg/cm, layer thickness $h_{fix}=20$ nm, and the spacer thickness (distance between free and fixed magnetic layers) $h_{Cu}=4$ nm. Magnetization dynamics of the fixed layer induced by the magnetodipolar interaction between the free and fixed layers was fully taken into account. Further, we assumed that the fixed layer thickness is large enough to neglect the spin torque effect on this layer. However, the direction of the electron polarization used to compute the spin torque acting on the free layer, was always adjusted to the instantaneous local magnetization direction of the fixed layer.

In principle, one should also keep in mind that the magnetocrystalline anisotropy of $Co_{90}Fe_{10}$ is not small (cubic anisotropy with $K_{cub}=-5.6\cdot10^5$ erg/cm^3) and hence, generally speaking, cannot be neglected. However, the influence of this anisotropy for a polycrystalline $Co_{90}Fe_{10}$ material as used in Ref. 14 is partially "averaged out"[38] due to the very small grain size (~10–20 nm). Both for this reason and lacking the exact knowledge about the grain size and texture of magnetic layers studied experimentally in Ref. 14, we present here only the results where the magnetocrystalline anisotropy of the fixed layer is neglected. Our preliminary studies show that when this random anisotropy is taken into account, a substantial dependence of the results on the grain size and film texture is observed, so that one should possess quantitative information about these parameters in order to make a meaningful quantitative comparison of simulated and experimental data. In order to study solely the effect of the magnetodipolar interaction between the fixed and free layers, we have also neglected the influence of the Oersted field in simulations which results are presented in this subsection.

The first very important result of our simulations is that the magnetodipolar interlayer interaction leads to the drastic reduction of the threshold current I_{th} for the magnetization oscillations onset: from the comparison of oscillation power plots in Fig. 10 it follows that the presence of the hard magnetic underlayer reduces the threshold current from $I_{th}\approx13$ mA for the single-layer system to ≈8 mA for the trilayer. The current where the transition from the propagating to localized modes occurs, is reduced from $I_{loc}\approx20$ mA for the single Py layer system to $I_{loc}\approx12$ mA (i.e., it nearly halves) when the presence of the CoFe underlayer is taken into account.

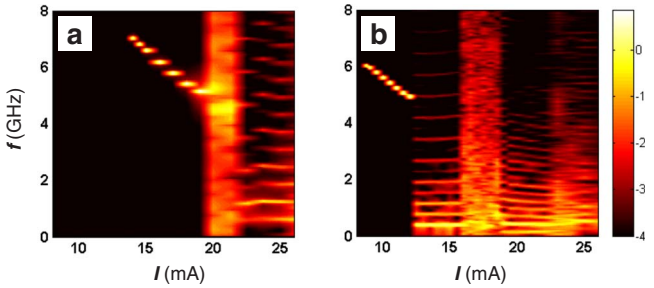

FIG. 10. (Color online) Comparison of spectral power maps of the m_z-component for the single-layer (a) and trilayer (b) systems ($\mathbf{H}_{Oe}=0$). The strong reduction of the current strength for the oscillation onset and for the transition to the localized modes due to the influence of the hard magnetic layer can be clearly seen (the discrete character of the $f(I)$ dependence for W-modes is due to the same reasons as explained in Fig. 2).

The most probable qualitative explanation of this effect is the following: when the magnetization of the free layer deviates slightly from its in-plane orientation (under the influence of the spin torque within the point-contact area), a stray field is generated. Straightforward geometrical consideration shows that this stray field causes the deviation of the fixed layer magnetization in the direction opposite to that of the free layer. This, in turn, results in the stronger deviation of the free layer magnetization due to the influence of the fixed layer stray field, thus leading to the positive feedback between the magnetization dynamics of the free and fixed layer. Such a positive feedback leads to the decrease in the threshold current for the oscillation onset. An additional decrease in the transition current from the propagating to the localized modes can be explained by the fact that magnetodipolar interlayer interaction field is strongly inhomogeneous, thus favoring the appearance of the localized modes. From the quantitative point of view, however, such a large decrease in the threshold current due to the magnetodipolar interlayer interaction is surprising.

Now we proceed to the discussion of the hard magnetic layer influence on various oscillation modes. As it can be seen from Fig. 10(b), for the trilayer system the first appearing mode (for currents slightly higher than $I_{th}\approx8$ mA) is also the propagating one. The pattern of the spatial wave propagation for this mode is asymmetric (see Fig. 11), which in this case is due to the inhomogeneous magnetodipolar field created by the hard magnetic layer (we recall that the Oersted field is not included into the trilayer simulations in order to isolate the interlayer interaction effect). The frequency at the oscillation onset is substantially lower than for a single-layer system (~6 GHz instead of ~7 GHz), showing that the interlayer interaction should be also taken into account, if the quantitative comparison between simulated and experimental frequencies is aimed. When the current increases further, the oscillation frequency decreases almost linearly with current, as for a single-layer system.

At the current value $I_{th}^{loc}\approx12.3$ mA we find a transition to the first localized mode of the trilayer (L_5 mode) with a very low (for the SPC-induced magnetization dynamics) frequency ~380 MHz. Similar to the L_1 mode of a single layer, the main dynamic process for this mode is the rotation of a

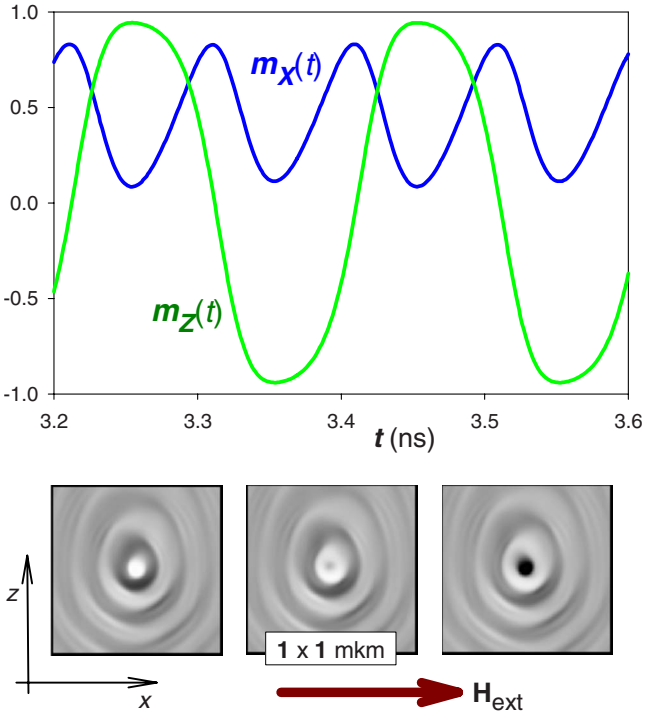

FIG. 11. (Color online) The same as in Fig. 3 for the propagating mode in the trilayer system for $\mathbf{H}_{\mathrm{Oe}}=0$.

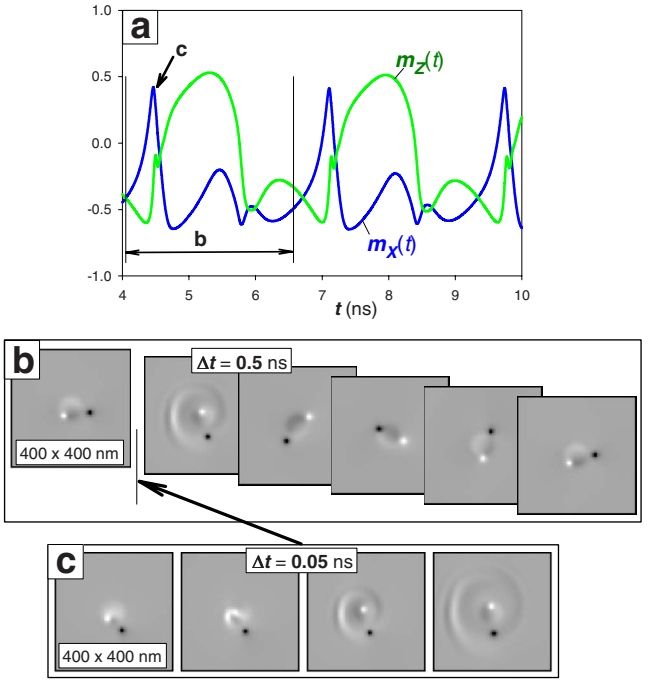

FIG. 12. (Color online) Magnetization time dependencies (a) and snapshots of the magnetization configurations (b) and (c) for low-current localized mode L_5 in the trilayer system ($\mathbf{H}_{\mathrm{Oe}}=0$). Panel (b) shows the rotation of the main vortex-antivortex pair (images of the out-of-plane magnetization component) and panel (c) illustrates the creation and annihilation of a satellite V-AV pair accompanied by the emitting of a spin-wave burst. Time intervals corresponding to the image rows of (b) and (c) are marked with vertical lines on the plot in the panel (a).

V-AV pair with opposite polarities of the vortex and antivortex [Fig. 12(b)]. During this rotation the V-AV distance slowly changes due to the interaction with the hard magnetic layer and presence of a small constant external field. However, in contrast to the L_1-mode for a single-layer case, here we observe during the rotation of this main V-AV pair the creation of a small (satellite) V-AV pair with *opposite* vortex and antivortex polarities. For this reason this small pair does not propagate (like the satellite pair for the L_1-mode), but its antivortex immediately annihilates with the vortex of the main pair, emitting a burst of spin waves [Fig. 12(c)], similar to localized modes found in the presence of the Oersted field [see Figs. 8(b) and 9]. This very fast creation-annihilation process manifests itself in a small cusp on the time dependence of the m_z projection and a large peak on $m_x(t)$ [Fig. 12(a)]. Due to the extremely anharmonic time dependencies of both these projections the oscillation power spectrum of the L_5 mode contains very strong higher harmonics clearly visible in Fig. 10(b).

When the current increases above ≈ 16 mA, magnetization dynamics becomes less regular, which manifests itself in a quasicontinuous power spectrum up to the current value ≈ 19 mA, where the next regular dynamic mode (L_6) appears. The major spectral peak of this mode has approximately the same frequency $f \approx 0.38$ GHz as for L_5, but the analysis of the magnetization configurations reveals that the complete period of m_z oscillations $T_z \approx 7.8$ ns corresponds to an ever lower frequency $f_z \approx 0.13$ GHz; corresponding relatively weak spectral band can be also seen in Fig. 10(b).

This high-current mode is the most complicated among regular modes studied here and combines all the processes analyzed above (see Fig. 13). Its formation starts from the nearly homogeneous magnetization deviation under the point-contact area, which evolves very rapidly into a V-AV pair with the same polarities of the vortex and antivortex (Fig. 13, image row A). This process is up to some extent similar to the formation of the high-current mode L_2 for a single-layer system (Fig. 5), but in the single-layer case *two* V-AV pairs were formed.

During the next stage (row B in the same figure) the V-AV distance in this pair increases, and the pair orientation is slightly changed, what is possible due to the magnetodipolar field of the hard layer (as mentioned above, the V-AV pair with the same V-AV polarities could move only translationally in the absence of external fields). At the third stage (row C in Fig. 13) the smaller V-AV pair is formed near the vortex of the main pair. The polarities of vortex and antivortex in this satellite pair are the same, but *opposite* relative to the V-AV polarities of the main pair. For this reason the antivortex of the new satellite pair annihilates very fast with the vortex of the main pair, emitting a burst of spin waves, as explained above.

As a result of this annihilation, the V-AV pair with nearly the same V-AV distance as at the very beginning of the process, but *opposite* polarities of vortex and antivortex, is left. Due to opposite V-AV polarities, this pair starts to rotate (row D in Fig. 13), and the distance between vortex and antivortex continuously decreases (probably also due to the influence of the underlayer stray field), until they annihilate (row E). The nearly homogeneous magnetization deviation under the

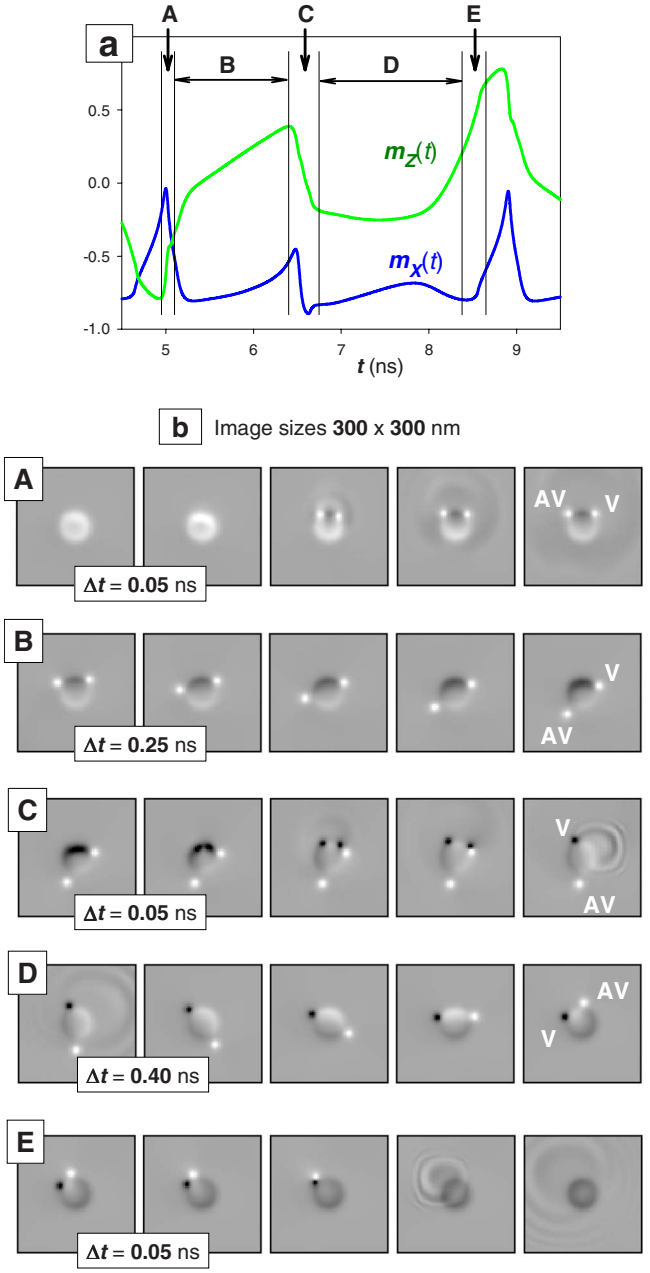

FIG. 13. (Color online) The same as in Fig. 12 for the high-current localized mode L_5 in the trilayer system ($\mathbf{H}_{Oe}=0$). Panels A–E show various dynamic processes constituting this very complicated mode; see text for details. Corresponding time intervals are marked on the plot in panel (a).

point-contact area left after this annihilation is directed *opposite* to the initial deviation at the start of the process. This means that the images displayed in the rows A-E in Fig. 13 correspond to a half of the complete magnetization dynamic period of this mode.

We would also like to emphasize that for all localized modes found in the system when the Oersted field was neglected (L_1, L_2, L_5, and L_6), the mode frequency was nearly independent on the current strength, although some of these modes existed in a quite large current region (e.g., modes L_5 and L_6). The most probable explanation of this interesting feature is that the mode frequency is determined by the rotation frequency of the V-AV pair(s) constituting the mode. This rotation frequency, in turn, is governed by the V-AV separation within the pair, which in our system is defined mainly by the point-contact diameter flooded by the current (in the absence of the Oersted field) and additionally—by the stray field of the underlayer (for the trilayer system). For this reason the mode frequency does not change noticeably with the current strength. The increasing amount of energy pumped into the system when the current strength grows is probably "consumed" during the process of the creation annihilation of satellite V-AV pairs discussed above. Indeed, a micromagnetic analysis has shown that the magnetization configuration of these pairs depends on the currents strength.

When the Oersted field is included, and it is large enough, the antivortex becomes immobile, and the mode frequency is determined by the oscillation of the vortex position within the potential well created by the Oersted field. For this reason the mode frequency increases with current, because larger currents create stronger Oersted fields. This frequency increase is especially pronounced for large κ (panel for $\kappa=0.5$ in Fig. 6),

D. Comparison with experimental results

At present there exist only very few experimental studies (partially supported by numerical simulations) of the SPC-driven microwave oscillations in the point-contact geometry, where it is proven—or at least suggested with a high plausibility degree—that this dynamics is governed by the vortex/antivortex motion.[14,24,25] Since we have chosen our simulation parameters according to the device characteristics from Ref. 14, we shall mainly compare our results with those reported in this paper.

First we note that we have simulated the in-plane field geometry, so that our results should be compared with the experimental data reported in the first part and in Fig. 1 of Ref. 14. It also follows from our simulations that for this particular setup, the strong influence of the interlayer interaction on the power spectra of the microwave oscillations cannot be neglected (see Sec. III C above). Hence only simulated data obtained for the complete trilayer system (see Fig. 10) can be used for a meaningful comparison with the experiment.

This comparison shows that our simulation results for the first localized mode of the trilayer (mode L_5, see Fig. 12) could reproduce semiquantitatively several important features of the real experiment. First, the current region where this mode is observed experimentally ($\Delta I_{exp}\approx 6-12$ mA) (see Fig. 1 in Ref. 14) is close to the region where our L_5 mode is found numerically ($\Delta I_{sim}\approx 12-16$ mA). The frequency of the experimentally observed microwave oscillations $f_{exp}\approx 100-220$ MHz (Ref. 14) is of the same order of magnitude as the simulated frequency $f_{sim}\approx 380$ MHz. Next, the weak dependence of the experimentally measured frequency on the current strength corresponds fairly well to our observation that the frequency of the localized modes for a trilayer is nearly current independent. Finally, the strongly nonsinusoidal character of simulated magnetization oscilla-

tions is in accordance with the presence of several higher harmonics in the experiment.[14]

The comparison of experiment and simulations could be more meaningful, if a better characterization of the experimentally studied system would be available. The problem is not only that several important geometric parameters (e.g., the point-contact diameter) are not known exactly. We have also found that the threshold current I_{th} for the oscillation onset depends on the average characteristics of the crystallographic structure of the hard layer (grain size and texture), and, what is less evident—that I_{th} is also different for various particular realizations of a random grain structure with the same average parameters. This difference is caused by substantial variations of the equilibrium magnetization configuration of the hard layer for various random grain structure realizations. The oscillation frequency itself and even the type of the first localized mode also depend on the crystallographic structure of the hard layer; it is worth noting here that the fundamental frequency of, e.g., our L_6 mode ($f_6 \approx 130$ MHz), lies within the experimentally measured frequency range.

Further, we have observed that when the Oersted field is taken into account (even strongly weakened with respect to a maximal possible field of an infinitely long nanowire), the type of the first localized mode could be changed. The Oersted field also causes the increase in the oscillation frequency with current similar to the frequency behavior observed experimentally.

There exist, however, important issues, where we observe a qualitative disagreement with experimental findings. The most important one is the presence of several well-defined different oscillation modes in the simulated dynamics, whereby experimentally only one oscillation mode was found (this statement is based mainly on the absence of any jumps on the current dependencies of the oscillation frequency and power). The absence of other localized modes at currents higher than the 'switch-off' current for the first localized mode in the experiment can be in principle explained as follows: according to Ref. 14, when the current is increased, the well-defined spectral peak evolves into "a broader band spectral output at larger current." This observation is consistent with the spectrum evolution found in our simulations, as demonstrated by the transition from a spectrum consisting of sharp spectral lines to a broad-band spectrum at $I \approx 16$ mA in Fig. 10(b). The next localized mode could be suppressed in a real experiment, because it emerges at much larger currents, when the sample heating and/or spin torque fluctuations due to the high spin current density prevents the formation of a well-defined oscillation mode.

The absence of the propagating mode (W-mode) is more difficult to explain. To try to understand why the W mode is absent in the experiment,[14] we first recall that the same discrepancy was found for systems with a small contact diameter in high fields. In simulations made for such systems for *increasing* current, the propagating mode emerged first,[21,22] and the localized ("bullet") mode appeared at higher currents[20]). However, experimentally only a localized mode was found.[12] The probable explanation of this contradiction was based on the theory of Slavin *et al.*,[20,26] according to which the threshold current I_{th}^{L} for the "bullet" mode is smaller than I_{th}^{W} for the W mode, but the "bullet" mode has the finite (and not even small) magnetization oscillation amplitude already at its threshold. For these reason the 'bullet' mode was not observed in simulations made for *increasing* current at $T=0$. These arguments were supported by numerical simulations (see detailed discussion in Refs. 21, 22, and 26), and it was suggested that in systems with a small contact diameter in high fields, the energy required to excite the localized mode with a finite amplitude is supplied by thermal fluctuations. These fluctuations excite the L mode at its threshold current I_{th}^{L}, which is smaller than I_{th}^{W} for the W-mode, so that the latter did not emerge at all. Whether this explanation is applicable to our case, where the current-flooded area is much larger—so that both thermal energy and the energy for a V-AV pair formation are higher—should be a subject of further studies.

Another problem which we have encountered is the reproduction of the experimentally observed hysteretic behavior of magnetization oscillations when the current was first *increased* to the value where the well-defined mode disappeared and then *decreased* to zero.[14] We could not reliably confirm this observation in our simulations, because we have found that the hysteretic behavior simulated numerically depends on the rate with which the current is decreased (this was not the case for systems with smaller point-contact diameter in high external fields). Due to the computer time limitations we had to decrease the current strength from its maximum to the value for which we intended to study the magnetization dynamics within $t_{red} \sim 10$ ns. Such interval was not enough to achieve results stable with respect to further increase in t_{red}. Experimentally, where the current is reduced within a macroscopic time interval, the corresponding problem obviously does not exist.

Comparison with other reports on the SPC-induced magnetization dynamics in the point-contact geometry[24,25] is possible only qualitatively, because systems studied in these papers considerably differ from our system. The paper of Mistral *et al.*[25] also deals with the magnetization dynamics for the point-contact injection in an extended thin-film sample, but the contact diameter used there is much larger ($d \approx 200$ nm) and the applied field is out of plane and relatively strong ($H_{perp} \approx 2000$ G). According to simulations from Ref. 25) this field leads to a formation of a single vortex already without any current. When the spin-polarized dc current is applied to this configuration, the vortex is driven out of the point-contact area. Its precession around this area governs the magnetization dynamics observed numerically and (most probably) experimentally. Because this dynamics is dominated by a single vortex motion, results of Ref. 25 cannot be directly compared to ours.

Finocchio *et al.*[24] recently studied magnetization oscillations in a multilayer nanopillar device with the elliptical cross section and small lateral dimensions 250×150 nm^2. The current was injected into the nanopillar via a point contact with the diameter $d \approx 40$ nm. Magnetization oscillations with the frequency $f \approx 0.8$ GHz were observed experimentally for zero and small applied fields, whereby the oscillation frequency was nearly current independent. Supporting numerical simulations[24] have shown that under these conditions the creation and subsequent rotation of a single V-AV

pair (analogous to our simplest localized modes discussed in detail above) can take place with a frequency quite close to the experimental value. The simulated rotation frequency of this pair also was almost independent on the current, in a qualitative agreement with our findings. However, a more detailed comparison of our data with the results from Ref. 24 is not really meaningful. First, the small lateral size of the nanopillar device studied in Ref. 24 is important by itself, strongly changing, e.g., conditions for the existence of a propagating mode. Second, the large shape anisotropy of this system may qualitatively affect the magnetization dynamics of localized modes. Here we would like only to mention that the absence of other dynamic modes and processes of the creation annihilation of satellite V-AV pairs (found by us for an extended thin-film geometry) is most probably due to this small lateral size of the nanopillar studied in Ref. 24.

IV. CONCLUSION

We have presented a detailed study of the magnetization dynamics induced by a spin-polarized current injected via a point contact into an extended magnetic multilayer for the case, when the point-contact diameter (D_c=80 nm) is relatively large compared to systems studied previously[12,13,20–23] and the in-plane external field (H_0=30 Oe) is very small. Under these conditions the system exhibits a rich variety of well-defined oscillation modes, which can be divided into propagating and localized ones.

The frequency of *propagating* modes in the simplest case (when the Oersted field and magnetodipolar interaction between the "free" and "fixed" layers are neglected) can be satisfactory described by the Slonczewski theory.[18,31] However, the agreement between simulated and analytically predicted threshold currents is significantly worse than for the point contact with the much smaller diameter (D_c=40 nm, see Refs. 21, 22, and 31). We assume that this is due to the strong anisotropy of the group velocity of spin waves, emitted out of the point-contact area for the low external field and large point-contact diameter (both factors lead to relatively low oscillation frequencies). Inclusion of the Oersted field and/or interlayer interaction narrows the current region for the existence of propagating modes and results in an asymmetric wave propagation pattern. This asymmetry is due not only to the Oersted and/or "fixed" layer stray fields on the spin-wave propagation itself, but also due to the deformation of the equilibrium magnetization configuration of the "free" layer by these fields.

When the Oersted field is neglected, *localized* modes for the system studied here are governed by the rotational and translational movement of V-AV pairs, in contrast to the small contact diameter case, where the dominating mode was the nonlinear "bullet.[20–22]" The simulated rotation frequency (for pairs with opposite polarities of V and AV) and translational motion velocity (for pairs with the same polarities of V and AV) for the *steady-state* motion of the V-AV pairs are in a good quantitative agreement with the theory of Komineas *et al.*,[34,35] which employs the scaling arguments familiar from the nonlinear dynamics. However, the actual dynamic modes involve much more complicated processes, in particular, the creation/annihilation of additional satellite V-AV pairs (which seem to play an important role for the energy emission out of the point-contact area) and creation/annihilation of the V-AV quadrupoles. These processes obviously require further investigation to achieve their deeper understanding.

We have also shown that the inclusion of the Oersted field can lead to qualitative changes of magnetization oscillation modes. In particular, for sufficiently large Oersted fields, the dynamics of V-AV localized modes are dominated by the oscillation of vortex in the potential well created by the Oersted field, whereby the antivortex is nearly immobile. This offers (in principle) a possibility to control the dominating magnetization dynamic mode by adjusting the electric contact setup, which is responsible for the Oersted field strength and configuration.

Finally, we have demonstrated that the magnetodipolar interlayer interaction is qualitatively important for the understanding of the magnetization dynamics in point-contact systems at low external fields, leading both to a strong decrease in the threshold current for the oscillation onset and to qualitative changes in the observed magnetization oscillation modes.

ACKNOWLEDGMENTS

We thank J. Miltat and S. Komineas for fruitful discussions.

[1] J. C. Slonczewski, J. Magn. Magn. Mater. **159**, L1 (1996).
[2] L. Berger, Phys. Rev. B **54**, 9353 (1996).
[3] J. Z. Sun, J. Magn. Magn. Mater. **202**, 157 (1999); M. Tsoi, A. G. M. Jansen, J. Bass, W.-C. Chiang, M. Seck, V. Tsoi, and P. Wyder, Phys. Rev. Lett. **80**, 4281 (1998).
[4] Y. Tserkovnyak, A. Brataas, G. E. W. Bauer, and B. I. Halperin, Rev. Mod. Phys. **77**, 1375 (2005).
[5] M. D. Stiles and J. Miltat, *Spin Transfer Torque and Dynamics*, Spin Dynamics in Confined Magnetic Structures III: Topics in Applied Physics 101 (Springer-Verlag, Berlin, Heidelberg, 2006).
[6] M. D. Stiles, in *Theory of Spin-Transfer Torque*, Handbook of Magnetism and Advanced Magnetic Materials, edited by H. Kronmüller and S. Parkin (JohnWiley & Sons, Ltd., Chichester, UK, 2007), Vol. 2.
[7] D. C. Ralph and M. D. Stiles, J. Magn. Magn. Mater. **320**, 1190 (2008).
[8] W. H. Rippard and M. R. Pufall, in *Microwave Generation in Magnetic Multilayers and Nanostructures*, Handbook of Magnetism and Advanced Magnetic Materials, edited by H. Kronmüller and S. Parkin (JohnWiley & Sons, Ltd., Chichester, UK, 2007), Vol. 2.

[9] F. B. Mancoff and S. Kaka, *Microwave Excitations in Spin Momentum Transfer Devices*, Handbook of Magnetism and Advanced Magnetic Materials, edited by H. Kronmüller and S. Parkin (John Wiley & Sons, Ltd., Chichester, UK, 2007), Vol. 5.
[10] T. J. Silva and W. H. Rippard, J. Magn. Magn. Mater. **320**, 1260 (2008).
[11] J. A. Katine and E. E. Fullerton, J. Magn. Magn. Mater. **320**, 1217 (2008).
[12] W. H. Rippard, M. R. Pufall, S. Kaka, S. E. Russek, and T. J. Silva, Phys. Rev. Lett. **92**, 027201(R) (2004).
[13] W. H. Rippard, M. R. Pufall, S. Kaka, T. J. Silva, and S. E. Russek, Phys. Rev. B **70**, 100406(R) (2004).
[14] M. R. Pufall, W. H. Rippard, M. L. Schneider, and S. E. Russek, Phys. Rev. B **75**, 140404(R) (2007).
[15] W. H. Rippard, M. R. Pufall, M. L. Schneider, K. Garello, and S. E. Russek, J. Appl. Phys. **103**, 053914 (2008).
[16] F. B. Mancoff, N. D. Rizzo, B. N. Engel, and S. Tehrani, Nature (London) **437**, 393 (2005).
[17] S. Kaka, M. R. Pufall, W. H. Rippard, T. J. Silva, S. E. Russek, and J. A. Katine, Nature (London) **437**, 389 (2005).
[18] J. C. Slonczewski, J. Magn. Magn. Mater. **195**, 261 (1999).
[19] D. V. Berkov, J. Magn. Magn. Mater. **300**, 159 (2006).
[20] A. Slavin and V. Tiberkevich, Phys. Rev. Lett. **95**, 237201 (2005).
[21] G. Consolo, B. Azzerboni, G. Gerhart, G. A. Melkov, V. Tiberkevich, and A. N. Slavin, Phys. Rev. B **76**, 144410 (2007).
[22] D. V. Berkov and N. L. Gorn, Phys. Rev. B **76**, 144414 (2007).
[23] D. V. Berkov, N. L. Gorn, J. Appl. Phys. **99**, 08Q701 (2006).
[24] G. Finocchio, O. Ozatay, L. Torres, R. A. Buhrman, D. C. Ralph, and B. Azzerboni, Phys. Rev. B **78**, 174408 (2008).
[25] Q. Mistral, M. van Kampen, G. Hrkac, and Joo-Von Kim, T. Devolder, P. Crozat, C. Chappert, L. Lagae, and T. Schrefl, Phys. Rev. Lett. **100**, 257201 (2008).
[26] D. V. Berkov and N. L. Gorn, J. Phys. D **41**, 164013 (2008).
[27] D. V. Berkov and J. Miltat, J. Magn. Magn. Mater. **320**, 1238 (2008).
[28] J. Pelzl, R. Meckenstock, D. Spoddig, F. Schreiber, J. Pflaum, and Z. Frait, J. Phys.: Condens. Matter **15**, S451 (2003).
[29] D. V. Berkov and N. L. Gorn, MICROMAGUS, package for micromagnetic simulations (http://www.micromagus.de).
[30] I. N. Krivorotov, D. V. Berkov, N. L. Gorn, N. C. Emley, J. C. Sankey, D. C. Ralph, and R. A. Buhrman, Phys. Rev. B **76**, 024418 (2007).
[31] A. N. Slavin and P. Kabos, IEEE Trans. Magn. **41**, 1264 (2005).
[32] A. Slavin and V. Tiberkevich, IEEE Trans. Magn. **44**, 1916 (2008).
[33] O. Tchernyshyov and G.-W. Chern, Phys. Rev. Lett. **95**, 197204 (2005).
[34] S. Komineas, Phys. Rev. Lett. **99**, 117202 (2007).
[35] S. Komineas, and N. Papanicolaou, arXiv:0712.3684 (unpublished).
[36] J. Miltat, *Spin Transfer: Towards a Fair Estimate of the Oersted Field in Pillar-like Geometries*, Talk on International Colloquium on Ultrafast Magnetization Processes, Irsee, Germany, Sept. 2008 (unpublished).
[37] R. Hertel and C. M. Schneider, Phys. Rev. Lett. **97**, 177202 (2006).
[38] K. Suzuki and G. Herzer, in *Advanced Nanomagnetic Structures*, edited by D. Sellmyer and R. Skomski (Springer, 2006), p. 365.